

Functionalized magnetite / silica nanocomposite for oily wastewater treatment

Seyfollah Gilak Hakimabadi¹, Ali Ahmadpour^{*1},
Mohammad T. Hamed Mosavian¹ and Tahereh Rohani Bastami^{1,2}

¹ Department of Chemical Engineering, Ferdowsi University of Mashhad, Mashhad, Iran

² Department of Chemical Engineering, Quchan University of Advanced Technology,
P.O. Box Quchan, 94771-67335, Iran (Current Address)

(Received March 28, 2015, Revised May 07, 2015, Accepted May 20, 2015)

Abstract. A new magnetite-silica core/shell nanocomposite ($\text{Fe}_3\text{O}_4@\text{nSiO}_2@\text{mSiO}_2$) was synthesized and functionalized with trimethylchlorosilane (TMCS). The prepared nanocomposite was used for the removal of diesel oil from aqueous media. The characterization of magnetite-silica nanocomposite was studied by X-ray diffraction (XRD), Fourier transform infrared (FTIR), transmission electron microscopy (TEM), surface area measurement, and vibrating sample magnetization (VSM). Results have shown that the desired structure was obtained and surface modification was successfully carried out. FTIR analysis has confirmed the presence of TMCS on the surface of magnetite silica nanocomposites. The low-angle XRD pattern of nanocomposites indicated the mesoscopic structure of silica shell. Furthermore, TEM results have shown the core/shell structure with porous silica shell. Adsorption kinetic studies indicated that the nanocomposite was able to remove 80% of the oil contaminant during 2 h and fit well with the pseudo-second order model. Equilibrium studies at room temperature showed that the experimental data fitted well with Freundlich isotherm. The magnetic property of nanocomposite facilitated the separation of solid phase from aqueous solution.

Keywords: magnetite silica nanocomposite; core-shell; oily pollutant; adsorption; functionalized surface

1. Introduction

Over recent years most waters have become increasingly polluted by oil. A large amount of oil spills into the aquatic ecosystem can cause serious environmental problems, including clogging of sewage treatment plants, adversely affecting the aquatic biota, and increasing biochemical oxygen demand due to large amount of bacteria necessary to decompose the oil (Wang *et al.* 2010a). The most frequent oils that are found in oily wastewater include lubricants, cutting oil, vegetable oil, light and heavy hydrocarbons. Major industrial sources of oily wastewater are petroleum refining and petrochemical plants, steel manufacturing and metal working, vehicle repair (Wang *et al.* 2012), and food processing.

*Corresponding author, Professor, E-mail: ahmadpour@um.ac.ir

Several techniques have been applied to remove oil including gravity-based separators, dissolved air flotation, electrocoagulation, biological treatment, and membrane filtration. Adsorption process has also been found as an effective method for the removal of oil from aqueous media. Oil adsorbents could generally be classified as polymeric (e.g., Polyacrylonitrile) (Ji *et al.* 2009), carbonic (e.g., Graphite, Activated carbon) (Ahmad *et al.* 2005b, Inagaki *et al.* 2000), inorganic (e.g., Bentonite, Silica aerogel) (Ahmad *et al.* 2005b, Wang *et al.* 2012), and biosorbents (e.g., Walnut shell, Barley straw) (Ibrahim *et al.* 2012, Srinivasan and Viraraghavan 2008).

Nanostructures such as magnetic nanocomposites (MNCs) are new materials which have recently been used in the field of wastewater treatment (Zhong *et al.* 2007, Syamimi Zaidi *et al.* 2014). Magnetic filtration is an emerging water treatment technology which can provide rapid and efficient removal of magnetic particles from wastewater stream (Ambashta and Sillanpää 2010). After the treatment, MNCs could be easily separated from the water media by using an external magnetic field. Different magnetic adsorbents were reported in the literature such as magnetic ion exchange resins (Kitis *et al.* 2007), magnetic zeolites (Oliveira *et al.* 2004), magnetic chitosan beads (Rorrer *et al.* 1993), magnetic activated carbon (Zhang *et al.* 2007), magnetic silica with core shell structure (Wang *et al.* 2010b), and magnetic nanoparticles impregnated agricultural wastes (Savina *et al.* 2011).

Recently, there have been increasing investigations about the exploitation of magnetic nanocomposites (MNCs) synthesized by embedding iron oxide nanoparticles (NPs) in organic (Oh and Park 2011), inorganic (Wang *et al.* 2010b), or hybrid (Abramson *et al.* 2011) matrices. Among different matrices, mesoporous silica has received considerable attention due to the promising properties of high surface area, ease of surface modification with different functional groups, biocompatibility, thermal and chemical stability (Delahaye *et al.* 2006).

Generally, magnetic iron oxide/silica nanocomposites (MSN) can be synthesized through the following procedures:

- (1) Initial wetness of the mesopores with iron oxide precursor, e.g. iron nitrate, and further calcination (Zhao *et al.* 2008).
- (2) Incorporation of iron oxide NPs into surface-modified mesoporous silica by impregnation (Deng *et al.* 2008).
- (3) Coating iron oxide NPs with a silica shell to form a magnetic core/silica shell structure (Hodgkins *et al.* 2007).

Usually, the first two approaches lead to pore blocking, thus decreasing the surface area of the magnetic nanocomposite. On the other hand, the third approach provides nanocomposites with larger surface area. Therefore, the core-shell structured MSN could be an efficient option for the adsorption process. Owing to their easy surface modification with different functional groups (Atia *et al.* 2009, Huang *et al.* 2013, Liu *et al.* 2012, Mahmoud *et al.* 2013, Niu *et al.* 2011, Xu *et al.* 2013), these MSNs have been used as adsorbents to remove various pollutants such as dyes (Faraji *et al.* 2010), heavy metals (Xu *et al.* 2013), and organic compounds (Atia *et al.* 2009). To the best of our knowledge, no research has been reported so far on the removal of oil from oily wastewater using the core-shell MSN.

In this work, we have fabricated a magnetic silica nanocomposite composed of a Fe_3O_4 core and two shells made of nonporous and mesoporous silica ($\text{Fe}_3\text{O}_4@n\text{SiO}_2@m\text{SiO}_2$), respectively. The magnetic characteristic of the Fe_3O_4 core allows the separation of MSN by applying a magnetic field. The first nonporous shell protects the core from oxidation and corrosion in harsh operating

conditions and also acts as a support for the second mesoporous shell which provides the surface area for the adsorption process (Xu *et al.* 2006). In order to remove oily pollutants, the surface of MSNs should be modified with hydrophobic groups. Organosilanes has frequently been used for the modification of mesoporous silica surface. However, few researches were reported the surface hydrophobization of core-shell MSNs using organosilanes (Atia *et al.* 2009). Here, we applied a reflux method and the surface modified by using Terimethylchlorosilane (TMCS). Characterization tests are subsequently performed on the products to investigate the formation of the desired Fe_3O_4 core-silica shell structure and also surface hydrophobicity. Finally, the adsorptive performance of MSNs for an oily pollutant is evaluated by conducting kinetic and equilibrium experiments.

2. Materials and methods

2.1 Chemicals

Iron(III) chloride hexahydrate ($\text{FeCl}_3 \cdot 6\text{H}_2\text{O}$), ethylene glycol anhydrous (EG), sodium acetate anhydrous (NaAc), tetraethyl orthosilicate (TEOS), terimethylchlorosilane (TMCS), cetyltrimethylammonium bromide (CTAB), ethenol (EtOH), ammonia solution, and triton X-100 were purchased from Merck Company. Diesel oil was supplied from a local fuel station.

2.2 Synthesis of Fe_3O_4 nanoparticles

The magnetic nanoparticles (MNPs) were prepared by a solvothermal method (Xu *et al.* 2006). Briefly, 1.35 g of $\text{FeCl}_3 \cdot 6\text{H}_2\text{O}$ was dissolved in 40 mL of ethylene glycol. Then, 3.60 g sodium acetate were added and stirred for 30 min at room temperature. The obtained homogeneous yellow solution was transferred to a Teflon-lined stainless-steel autoclave and sealed to heat at 180°C . After reaction for 12 h, the autoclave was cooled to room temperature. The obtained black magnetite particles were washed with acetone and water several times, and then dried at 50°C overnight.

2.3 Synthesis of $\text{Fe}_3\text{O}_4@n\text{SiO}_2@m\text{SiO}_2$ nanocomposite

The Fe_3O_4 nanoparticles were first coated with a thin nonporous silica layer through the sol-gel process (Deng *et al.* 2008). In brief, 0.1 g of Fe_3O_4 nanoparticles were treated with 0.1 M HCl aqueous solution (50 mL) in an ultrasonic bath for 10 min. Then, MNPs were separated by magnet and washed by deionized water. The treated MNPs were dispersed in the mixture of 80 mL ethanol and 20 mL deionized water and then mechanically stirred for 150 min. Subsequently, 1 mL of ammonia aqueous solution (28wt%) was added to the mixture at room temperature followed by addition of 0.1 g TEOS after 10 min. The mixture was stirred at room temperature for 6 h. Finally, the $\text{Fe}_3\text{O}_4@n\text{SiO}_2$ particles were separated by magnet and washed with acetone and water and then dried at 50°C overnight. To coat the $\text{Fe}_3\text{O}_4@n\text{SiO}_2$ with a mesoporous silica layer, $\text{Fe}_3\text{O}_4@n\text{SiO}_2$ particles were dispersed in a mixture containing 0.3 g CTAB, 80 mL deionized water and 60 mL ethanol and stirred for 3 h. 1 g of a 28wt% ammonia solution was also added. After 30 min, 0.4 g TEOS was added dropwise in 2-3 min and the mixture was stirred for 6 h. The obtained particles were washed with acetone and water and dried at 50°C overnight. Finally, the products were dispersed in 60 mL ethanol and stirred for 6 h at 60°C three times to extract the CTAB from the nanocomposite structure.

2.4 Surface modification of $Fe_3O_4@nSiO_2@mSiO_2$ nanocomposite

0.1 g of $Fe_3O_4@nSiO_2@mSiO_2$ composite was soaked in 50 mL of a solution containing 10wt% TMCS in toluene and allowed to react in reflux situation for 150 min. The modified products were washed with acetone several times and dried at 50°C overnight.

2.5 Characterization

The composition and crystal phase of the samples were characterized by low angle ($0.71 < 2\theta < 10$) and wide angle ($5 < 2\theta < 80$) X-ray diffraction (XRD) on a X'Pert Pro MPD X-ray diffractometer equipped with Cu irradiation ($\lambda = 1.5406\text{\AA}$). To determine size and morphology of the samples, transmission electron microscope (TEM) images were taken using a Philips CM120 electron microscope. Fourier transform infrared (FTIR) spectra of the samples were recorded on a Thermo Nicolet, Avatar 370 FTIR in the range of 400-4000 cm^{-1} . Surface area, pore size and pore volume were measured by a BEL-SORP-mini II (Japan) analyzer. The magnetic property of magnetite nanoparticle and magnetic AC was investigated using vibrating sample magnetometer (VSM), Leckeshore model. Oil concentration was determined by a WPA S2000 UV-Vis spectrophotometer.

2.6 Preparation of oil/water (O/W) emulsion

Certain amount of diesel oil was added to deionized water and Triton X-100 (0.1wt%) was used as an emulsifier to stabilize the emulsion. The obtained mixture was mechanically stirred to achieve a homogeneous emulsion. The resulting emulsion remained stable for at least one week.

2.7 Liquid phase adsorption

Kinetic experiments were conducted in a batch system using a magnetic stirrer at room temperature. About 20 mg of MSN was transferred to the reactor containing 10 mL of oil-in-water emulsions with 10 mgL^{-1} concentration at different contact times until the equilibrium was reached. MSN was separated using a magnet and the residual concentration of the oily pollutant was determined by UV-Vis spectroscopy at maximum absorbing wavelength ($\lambda = 220$ nm).

Batch isotherm experiments were also conducted at room temperature using 20 mg of MSN with different oil initial concentrations (10-50 mgL^{-1}) at the optimum time to reach equilibrium condition. All kinetic and isotherm experiments were duplicated. The oil uptake at equilibrium per unit gram of adsorbent, q_e (mgg^{-1}) was calculated by

$$q_e = \frac{(C_0 - C_e)V}{W} \quad (1)$$

C_e (mgL^{-1}) is the concentration of diesel oil in liquid-phase at equilibrium, C_0 (mgL^{-1}) is the initial concentration of diesel oil, V (L) is the sample volume, and W (g) is the mass of adsorbent.

2.8 Regeneration studies

20 mg of MSN was transferred to the reactor containing 10 mL of a 10 mgL^{-1} oil-in-water emulsion and stirred for 2 h, then was separated using a magnet. The spent MSN was dispersed in 8 mL hexane and mixed for 2 h. The adsorption capability of oil-extracted sample was then evaluated using the above procedure and this adsorption-desorption cycle was repeated 5 times.

3. Results and discussion

3.1 Characterization of MSNs

The wide-angle XRD patterns of as-synthesized Fe_3O_4 and $\text{Fe}_3\text{O}_4@n\text{SiO}_2@m\text{SiO}_2$ are shown in Fig. 1. The diffraction peaks at 2θ values of 18.5° , 30.3° , 35.7° , 43.3° , 53.7° , 57.2° , 62.8° , and 74.3° refer to (111), (022), (113), (004), (224), (115), and (044) planes of face center cubic magnetite (Fe_3O_4) phase (ICDD-98-001-2126, space group Fd-3m, $a = b = c = 8.34\text{\AA}$), respectively. These peaks are maintained after coating the Fe_3O_4 with two shells of SiO_2 (nonporous and mesoporous) which confirms that the Fe_3O_4 structure was not damaged. The XRD pattern of $\text{Fe}_3\text{O}_4@n\text{SiO}_2@m\text{SiO}_2$ exhibits a broad peak in the range of $2\theta = 15\text{--}30^\circ$, which is assigned to the amorphous SiO_2 . The low-angle XRD pattern of $\text{Fe}_3\text{O}_4@n\text{SiO}_2@m\text{SiO}_2$ (Fig. 1 insert) shows a reflection peak at about $2\theta = 2.5^\circ$, which indicates the short range mesoscopic ordering character of nanocomposite.

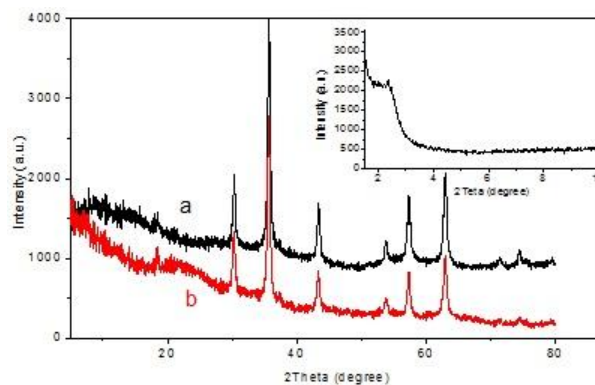
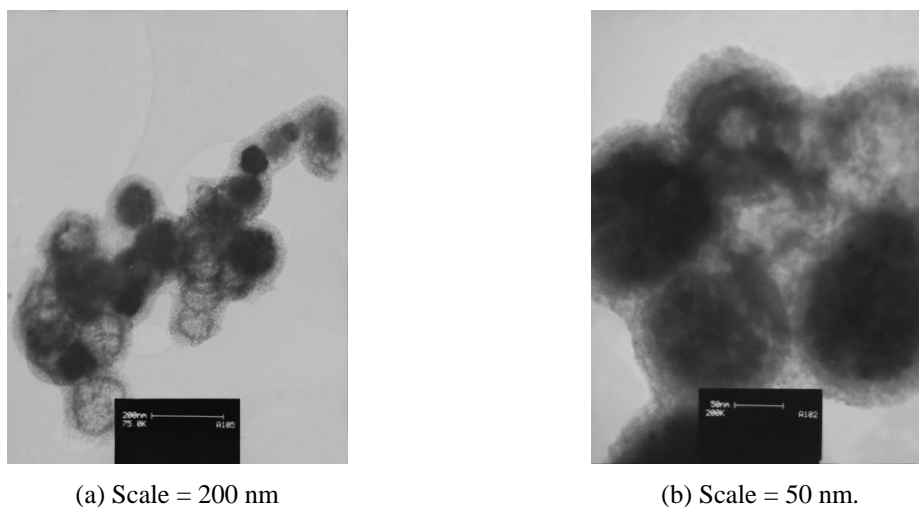


Fig. 1 Wide-angle XRD patterns for (a) Fe_3O_4 and (b) $\text{Fe}_3\text{O}_4@n\text{SiO}_2@m\text{SiO}_2$ and low-angle XRD patterns for functionalized $\text{Fe}_3\text{O}_4@n\text{SiO}_2@m\text{SiO}_2$ (insert)



(a) Scale = 200 nm

(b) Scale = 50 nm.

Fig. 2 TEM images of $\text{Fe}_3\text{O}_4@n\text{SiO}_2@m\text{SiO}_2$

Fig. 2 illustrates the core-shell structure of magnetic silica nanocomposites. It is clearly seen that iron oxide cores have a uniform size of 100-150 nm, which facilitates the separation of particles from the liquid media. Thickness of the first and the second shell is about 15 nm. Additionally, a few silica particles can be observed in Fig. 2(b), which are presumably as a result of insufficient washing.

Magnetization curve of prepared $\text{Fe}_3\text{O}_4@n\text{SiO}_2@m\text{SiO}_2$ at room temperature is shown in Fig. 3. As shown in this curve, the saturation magnetization and remanence for Fe_3O_4 are 62.7 emu.g^{-1} and 1.6 emu.g^{-1} and for MSN are 40.2 emu.g^{-1} and 0.8 emu.g^{-1} , respectively. In both cases, the remanences are close to zero and no hysteresis is observed. So, both samples can be separated easily in a suspended system. Furthermore, the nanocomposites can be re-dispersed after they are separated by an external magnetic field, which is due to their superparamagnetic behavior.

FTIR spectra of $\text{Fe}_3\text{O}_4@n\text{SiO}_2@m\text{SiO}_2$ before and after functionalization are shown in Figs. 4(a) and (b). The peaks around 580 cm^{-1} and 1089 cm^{-1} are attributed to Fe-O band of Fe_3O_4 and Si-O-Si band of silica shell, respectively. The peaks centered at 3450 cm^{-1} could be assigned to OH vibration and physisorbed water molecules, which was almost disappeared after functionalization due to the reaction of TMCS with OH groups leading to the replacement of $\text{O-Si(CH}_3)_3$ with $-\text{OH}$

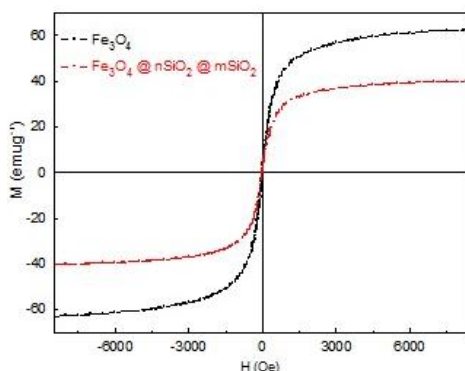


Fig. 3 The VSM curve of Fe_3O_4 and $\text{Fe}_3\text{O}_4@n\text{SiO}_2@m\text{SiO}_2$ composite

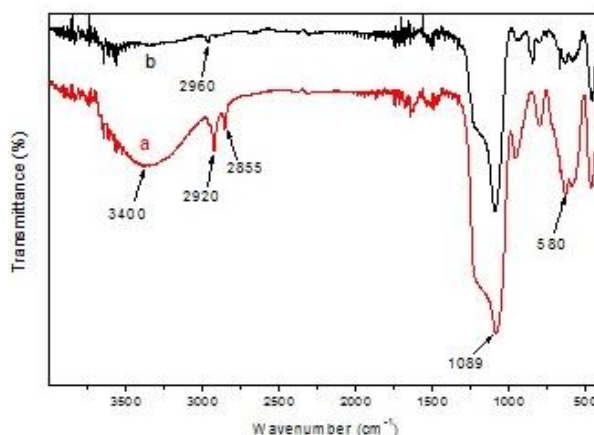


Fig. 4 The FTIR spectra of $\text{Fe}_3\text{O}_4@n\text{SiO}_2@m\text{SiO}_2$ (a) as-synthesized; and (b) after functionalization

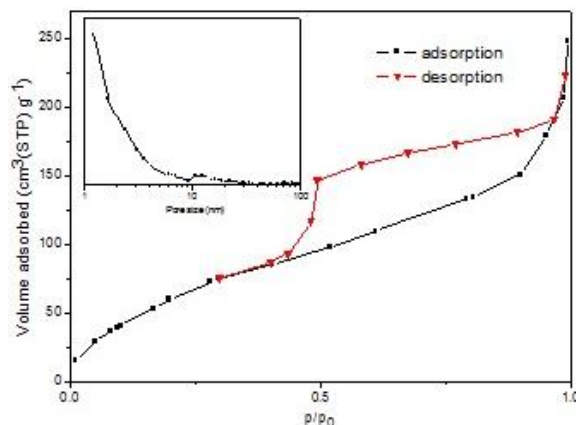


Fig. 5 N₂ adsorption-desorption isotherm and pore size distribution of functionalized Fe₃O₄@nSiO₂@mSiO₂ composite

groups. The two sharp peaks at 2920 cm⁻¹ and 2855 cm⁻¹ are assigned to C-H bands in CTAB which was used as a template to coat the Fe₃O₄@nSiO₂ with mesoporous silica. After functionalization, these peaks are disappeared because of the extraction of CTAB from the nanocomposite structure. Moreover, two new peaks can be seen around 2960 cm⁻¹ and 845 cm⁻¹ characteristics of C-H bands of methyl groups, which indicates that TMCS is attached to the surface and confirms the hydrophobic nature of the surface.

The N₂ adsorption-desorption isotherm for MSN exhibits type (IV) curve which is the characteristic of mesoporous material (Fig. 5). The BET surface area and total pore volume of MSN are 267.56 m².g⁻¹ and 0.3568 cm³.g⁻¹, respectively. Pore size distribution curve shows a sharp peak at 1.21 nm and a small peak at 10.65 nm, which indicates that the MSN structure is mainly composed of a complex network of micro and mesopores.

3.2 Adsorption kinetic studies

Fig. 6 shows the effect of contact time for the removal of diesel oil using magnetic nanosorbent. It can be seen that the equilibrium was reached within 2 h. The adsorption process can be divided into two distinct steps. Rate of adsorption was rapid in the first 45 min due to higher concentration gradient. The second step represents a significant decrease in adsorption rate because of approaching to the equilibrium. The removal of diesel oil at equilibrium was equal to 80%.

Numerous kinetic models have been proposed to describe the adsorption mechanism (Ho 2006). To analyze the adsorption kinetic models, the Lagergren pseudo-first order (Lagergren 1898) and McKay and Ho's pseudo-second order (Ho and McKay 1998) models were applied and the results showed that the experimental data fitted well to pseudo-second order equation.

Lagergren's model was the first adsorption rate equation based on the adsorption capacity for solid-liquid system. This model that is also called pseudo-first order model can be represented as

$$\log(q_e - q_t) = \log q_e - \frac{K_1 t}{2.303} \quad (2)$$

q_e and q_t are the amounts of adsorbate onto the sorbent (mg.g⁻¹) at equilibrium and time t ,

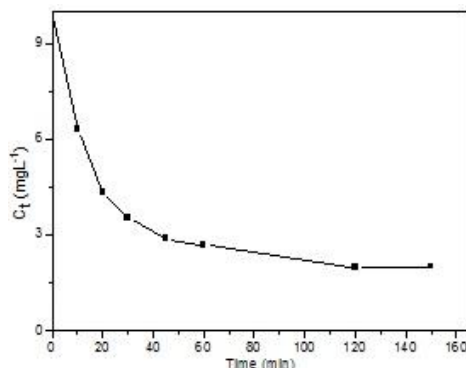


Fig. 6 Effect of contact time for the removal of diesel oil at room temperature (initial concentration = 10 mgL^{-1} , mass of sorbent = 20 mg, volume of effluent = 10 mL)

respectively, and K_1 is the rate constant of pseudo-first-order (min^{-1}) model.

Ho's equation or pseudo-second-order equation is another common model based on adsorption capacity which was first introduced for the kinetics of adsorption of divalent metal ions onto peat. If the adsorption rate is governed by this model, the rate controlling step would be chemisorption of diesel oil on the surface. Ho's equation can be expressed as

$$\frac{t}{q_e} = \frac{1}{K_2 q_e^2} + \frac{t}{q_e} \quad (3)$$

Where K_2 ($\text{g} \cdot (\text{mg} \cdot \text{min})^{-1}$) is the rate constant of second order adsorption. The slope and intercept of plots of t/q_t versus t (not shown) were used to calculate the second rate constant K_2 . The outputs of these equations are listed in Table 1. In the case of Lagergren's model, the correlation coefficient (R^2) is lower than 1 indicating that the adsorption process is not pseudo-first-order. On the contrary, Ho's model led to the R^2 about 0.9965, which suggest that this model can accurately predict the adsorption process and the rate controlling step is chemisorption. Moreover, the calculated q_e by the pseudo-second-order equation is approximately equal to q_e obtained from the experimental data, while the pseudo-first-order equation does not give precise value of q_e .

In order to describe the adsorption mechanism, the intraparticle diffusion model was also applied. According to this model, the adsorbed amount on the adsorbent is a function of $t^{1/2}$ as follows

$$q_t = K_{\text{int}} t^{0.5} + c \quad (4)$$

Where K_{int} is the intraparticle diffusion rate constant and c is the intercept. The K_{int} value can be

Table 1 Kinetic parameters for the adsorption of diesel oil onto MSN

| Lagergren's equation | | | | Ho's equation | | | |
|----------------------|-----------------------------|---|---|---------------|--|---|---|
| R_2 | K_1 (min^{-1}) | $q_{e,\text{exp.}}$ ($\text{mg} \cdot \text{g}^{-1}$) | $q_{e,\text{cal.}}$ ($\text{mg} \cdot \text{g}^{-1}$) | R_2 | K_2 ($\text{g} \cdot (\text{mg} \cdot \text{min})^{-1}$) | $q_{e,\text{exp.}}$ ($\text{mg} \cdot \text{g}^{-1}$) | $q_{e,\text{cal.}}$ ($\text{mg} \cdot \text{g}^{-1}$) |
| 0.9613 | 0.037 | 4 | 2.63 | 0.9965 | 0.017 | 4 | 4.52 |

obtained from the linear plots of q_t versus $t^{0.5}$. The values of c provide information about the thickness of the boundary layer, i.e., the larger the intercept, the greater the boundary layer effect (Kannan and Sundaram 2001).

Previous researches have shown that the plot of q_t vs. $t^{0.5}$ may compose of two or more linear portions, which means that two or more steps occur during the adsorption process. The first step is film diffusion which includes the adsorption of a component from liquid bulk onto the surface. The second step is the gradual adsorption in which intraparticle diffusion begins. The third portion is equilibrium stage where the rate of intraparticle diffusion decreases (Wu *et al.* 2000).

Fig. 7 depicts multi-linear correlation between q_t and $t^{0.5}$. It can be seen that there is two linear parts, suggesting that the whole adsorption process is not only affected by intraparticle diffusion but also the film diffusion occurs (Hu *et al.* 2011). As shown in Table 2, the slope of the first line ($K_{int,1}$) is higher than that of the second line ($K_{int,2}$) because the rate of intraparticle diffusion decreases as the adsorption process approaches the equilibrium.

3.3 Adsorption isotherm studies

Adsorption isotherm is essential for determining the adsorption capacity and analysis and design of the adsorption system (Keller and Staudt 2005). The most common isotherms applied in researches are Langmuir and Freundlich.

Langmuir model assumes that the adsorption is monolayer and the adsorption energy of all active sites is equal. Langmuir equation can be expressed in linear form as

$$\frac{1}{q_e} = \frac{1}{q_m} + \frac{1}{b q_m C_e} \tag{5}$$

Table 2 Rate constants of intraparticle diffusion model for the adsorption of diesel oil onto MSN

| $K_{int,1}$ (mg.g ⁻¹ .time ^{-0.5}) | $K_{int,2}$ (mg.g ⁻¹ .time ^{-0.5}) |
|---|---|
| 0.6012 | 0.1341 |

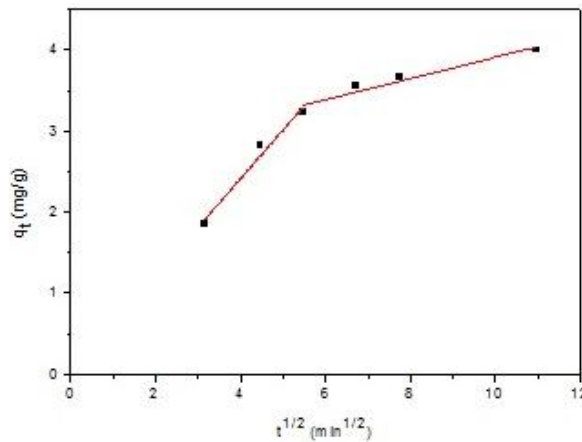


Fig. 7 Test of intraparticle diffusion model for adsorption of diesel oil onto MSN

Where C_e ($\text{mg}\cdot\text{L}^{-1}$) is the equilibrium concentration of the adsorbate, q_e ($\text{mg}\cdot\text{g}^{-1}$) is the amount of adsorbed per unit mass of adsorbent, q_m ($\text{mg}\cdot\text{g}^{-1}$) and b are Langmuir constants.

The essential features of Langmuir isotherm can be expressed in terms of dimensionless constant separation factor, R_L , which is obtained using the following equation (Ahmad *et al.* 2005a)

$$R_L = \frac{1}{(1 + K_L C_0)} \quad (6)$$

This factor determines the type of isotherm according to Table 3. In this work, R_L is between 0 and 1, indicating that the adsorption of diesel oil onto MSN is favorable. Freundlich equation is an empirical model which is established on the assumption of heterogeneous surface and multilayer adsorption (Davila-Jimenez *et al.* 2005). This model presumes that adsorption sites possess unequal energy. Freundlich isotherm is expressed as

$$q_e = K_F C_e^{\frac{1}{n}} \quad (7)$$

Where K_F is roughly an indicator of the adsorption capacity and $(1/n)$ is the adsorption intensity. Values of $n > 1$ represent a favorable adsorption condition. This equation can be rearranged in linear form by taking logarithm of Eq. (7) resulting

$$\log q_e = \log K_F + \frac{1}{n} \log C_e \quad (8)$$

The plot of $\log q_e$ vs. $\log C_e$ gives the values of n and K_F . The value of n is a measure of

Table 3 Type of isotherm in terms of R_L value

| R_L value | Type of isotherm |
|---------------|------------------|
| $R_L = 0$ | Irreversible |
| $0 < R_L < 1$ | Favorable |
| $R_L = 1$ | Linear |
| $R_L > 1$ | Unfavorable |

Table 4 Type of isotherm in terms of $1/n$ value

| $\frac{1}{n}$ value | Type of isotherm |
|-----------------------|------------------|
| $\frac{1}{n} = 0$ | Irreversible |
| $0 < \frac{1}{n} < 1$ | Favorable |
| $\frac{1}{n} > 1$ | Unfavorable |

Table 5 Parameters of Langmuir and Freundlich isotherms for the adsorption of diesel oil onto MSN

| Langmuir model | | | Freundlich model | | |
|----------------|---------------------------|-----------------------------|------------------|------|-------|
| R^2 | b (l.mg ⁻¹) | q_m (mg.g ⁻¹) | R^2 | n | K_f |
| 0.82 | 0.1 | 15.6 | 0.92 | 2.36 | 2.75 |

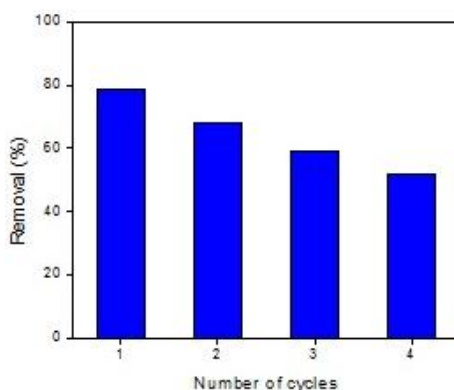


Fig. 8 Regeneration studies after 4 cycles

adsorption favorability according to Table 4. The constants obtained from fitting the experimental data with Langmuir and Freundlich isotherms are listed in Table 5. Comparing the correlation factors of these two models shows that the equilibrium data fit better with the Freundlich isotherm, which is presumably due to the fact that heterogeneity is considered in this model. In other words, the methyl groups resulted from the modification of the MSN surface are responsible for heterogeneity.

3.4 Regeneration studies

Good desorption performance of an adsorbent is important in its potential practical applications. The adsorption capacities of magnetic silica nanocomposites during adsorption / desorption cycles are shown in Fig. 8. It can be observed that the adsorption capacity remains constant only after first cycle. It was suggested that the reduction of adsorption capacity after two cycles was due to low desorption percentages of oily pollutants from hydrophobic surface of silica and confirmed the strongly adsorption of diesel oil onto surface of magnetic / silica nanocomposites.

4. Conclusions

The removal of diesel oil from an oil/water emulsion was carried out using adsorption of oil onto MSN with core-shell structure. The characterization tests indicated the formation of desired adsorbent with hydrophobic nature and acceptable adsorptive as well as magnetic properties. It can be proven from the batch kinetic studies that the adsorption process was rapid for the first 45 min and equilibrium was reached within 2 h in 10 mL volume of 10 mg.L⁻¹ concentration. Kinetic and equilibrium data fitted well with Ho's model and Freundlich isotherm, respectively. Regeneration studies showed that the performance of MSN was mostly maintained for one adsorption-

desorption cycle.

References

- Abramson, S., Safraou, W., Malezieux, B., Dupuis, V., Borensztajn, S., Briot, E. and Bée, A. (2011), "An eco-friendly route to magnetic silica microspheres and nanospheres", *J. Colloid Interface Sci.*, **364**(2), 324-332.
- Ahmad, A., Sumathi, S. and Hameed, B. (2005a), "Adsorption of residue oil from palm oil mill effluent using powder and flake chitosan: equilibrium and kinetic studies", *Water Res.*, **39**(12), 2483-2494.
- Ahmad, A., Sumathi, S. and Hameed, B. (2005b), "Residual oil and suspended solid removal using natural adsorbents chitosan, bentonite and activated carbon: A comparative study", *Chem. Eng. J.*, **108**(1), 179-185.
- Ambashta, R.D. and Sillanpää, M. (2010), "Water purification using magnetic assistance: A review", *J. Hazard. Mater.*, **180**(1), 38-49.
- Atia, A.A., Donia, A.M. and Al-Amrani, W.A. (2009), "Adsorption/desorption behavior of acid orange 10 on magnetic silica modified with amine groups", *Chem. Eng. J.*, **150**(1), 55-62.
- Davila-Jimenez, M., Elizalde-Gonzalez, M. and Peláez-Cid, A. (2005), "Adsorption interaction between natural adsorbents and textile dyes in aqueous solution", *Colloids and Surfaces A: Physicochem. Eng. Aspects*, **254**(1), 107-114.
- Delahaye, E., Escax, V., El Hassan, N., Davidson, A., Aquino, R., Dupuis, V., Perzynski, R. and Raikher, Y. (2006), "Nanocasting": using SBA-15 silicas as hard templates to obtain ultrasmall monodispersed γ -Fe₂O₃ nanoparticles", *J. Phys. Chem. B*, **110**(51), 26001-26011.
- Deng, Y., Qi, D., Deng, C., Zhang, X. and Zhao, D. (2008), "Superparamagnetic high-magnetization microspheres with an Fe₃O₄@SiO₂ core and perpendicularly aligned mesoporous SiO₂ shell for removal of microcystins", *J. Am. Chem. Soc.*, **130**(1), 28-29.
- Faraji, M., Yamini, Y. and Rezaee, M. (2010), "Magnetic nanoparticles: Synthesis, stabilization, functionalization, characterization, and applications", *J. Iran. Chem. Soc.*, **7**(1), 1-37.
- Ho, Y.-S. (2006), "Review of second-order models for adsorption systems", *J. Hazard. Mater.*, **136**(3), 681-689.
- Ho, Y.-S. and McKay, G. (1998), "Sorption of dye from aqueous solution by peat", *Chem. Eng. J.*, **70**(2), 115-124.
- Hodgkins, R.P., Ahnizay, A., Parekh, K., Belova, L.M. and Bergström, L. (2007), "Maghemite nanocrystal impregnation by hydrophobic surface modification of mesoporous silica", *Langmuir*, **23**(17), 8838-8844.
- Hu, X.-J., Wang, J.-S., Liu, Y.-G., Li, X., Zeng, G.-M., Bao, Z.-L., Zeng, X.-X., Chen, A.-W. and Long, F. (2011), "Adsorption of chromium (VI) by ethylenediamine-modified cross-linked magnetic chitosan resin: isotherms, kinetics and thermodynamics", *J. Hazard. Mater.*, **185**(1), 306-314.
- Huang, D., Sha, Y., Zheng, S., Liu, B. and Deng, C. (2013), "Preparation of phenyl group-functionalized magnetic mesoporous silica microspheres for fast extraction and analysis of acetaldehyde in mainstream cigarette smoke by gas chromatography-mass spectrometry", *Talanta*, **115**, 427-434.
- Ibrahim, S., Ang, H.M. and Wang, S. (2012), "Adsorptive separation of emulsified oil in wastewater using biosorbents", *Asia-Pacific J. Chem. Eng.*, **7**(S2), S216-S221.
- Inagaki, M., Konno, H., Toyoda, M., Moriya, K. and Kihara, T. (2000), "Sorption and recovery of heavy oils by using exfoliated graphite Part II: Recovery of heavy oil and recycling of exfoliated graphite", *Desalination*, **128**(3), 213-218.
- Ji, F., Li, C., Dong, X., Li, Y. and Wang, D. (2009), "Separation of oil from oily wastewater by sorption and coalescence technique using ethanol grafted polyacrylonitrile", *J. Hazard. Mater.*, **164**(2), 1346-1351.
- Kannan, N. and Sundaram, M.M. (2001), "Kinetics and mechanism of removal of methylene blue by adsorption on various carbons – A comparative study", *Dyes Pigments*, **51**(1), 25-40.
- Keller, J.U. and Staudt, R. (2005), *Gas Adsorption Equilibria: Experimental Methods and Adsorptive Isotherms*, Springer Science & Business Media, Boston, MA, USA.

- Kitis, M., Harman, B.I., Yigit, N.O., Beyhan, M., Nguyen, H. and Adams, B. (2007), "The removal of natural organic matter from selected Turkish source waters using magnetic ion exchange resin (MIEX®)", *React. Funct. Polym.*, **67**(12), 1495-1504.
- Largergren, S. (1898), "Zur theorie der sogenannten adsorption geloster stoffe. Kungliga Svenska Vetenskapsakademiens", *Handlingar*, **24**, 1-39.
- Liu, Z., Yang, H., Zhang, H., Huang, C. and Li, L. (2012), "Oil-field wastewater purification by magnetic separation technique using a novel magnetic nanoparticle", *Cryogenics*, **52**(12), 699-703.
- Mahmoud, M.E., Abdelwahab, M.S. and Fathallah, E.M. (2013), "Design of novel nano-sorbents based on nano-magnetic iron oxide-bound-nano-silicon oxide-immobilized-triethylenetetramine for implementation in water treatment of heavy metals", *Chem. Eng. J.*, **223**, 318-327.
- Niu, H.-Y., Li, W.-H., Shi, Y.-L. and Cai, Y.-Q. (2011), "A core-shell magnetic mesoporous silica sorbent for organic targets with high extraction performance and anti-interference ability", *Chem. Commun.*, **47**(15), 4454-4456.
- Oh, J.K. and Park, J.M. (2011), "Iron oxide-based superparamagnetic polymeric nanomaterials: design, preparation, and biomedical application", *Prog. Polym. Sci.*, **36**(1), 168-189.
- Oliveira, L.C., Petkowicz, D.I., Smaniotto, A. and Pergher, S.B. (2004), "Magnetic zeolites: a new adsorbent for removal of metallic contaminants from water", *Water Res.*, **38**(17), 3699-3704.
- Rorrer, G.L., Hsien, T.Y. and Way, J.D. (1993), "Synthesis of porous-magnetic chitosan beads for removal of cadmium ions from wastewater", *Ind. Eng. Chem. Res.*, **32**(9), 2170-2178.
- Savina, I.N., English, C.J., Whitby, R.L., Zheng, Y., Leistner, A., Mikhalovsky, S.V. and Cundy, A.B. (2011), "High efficiency removal of dissolved As (III) using iron nanoparticle-embedded macroporous polymer composites", *J. Hazard. Mater.*, **192**(3), 1002-1008.
- Srinivasan, A. and Viraraghavan, T. (2008), "Removal of oil by walnut shell media", *Bioresour. Technol.*, **99**(17), 8217-8220.
- Syamimi Zaidi, N., Sohaili, J., Muda, K. and Sillanpää, M. (2014), "Magnetic field application and its potential in water and wastewater treatment systems", *Sep. Purif. Rev.*, **43**(3), 206-240.
- Wang, D., Silbaugh, T., Pfeffer, R. and Lin, Y. (2010a), "Removal of emulsified oil from water by inverse fluidization of hydrophobic aerogels", *Powder Technol.*, **203**(2), 298-309.
- Wang, J., Zheng, S., Shao, Y., Liu, J., Xu, Z. and Zhu, D. (2010b), "Amino-functionalized Fe₃O₄@SiO₂ core-shell magnetic nanomaterial as a novel adsorbent for aqueous heavy metals removal", *J. Colloid Interface Sci.*, **349**(1), 293-299.
- Wang, D., McLaughlin, E., Pfeffer, R. and Lin, Y. (2012), "Adsorption of oils from pure liquid and oil-water emulsion on hydrophobic silica aerogels", *Sep. Purif. Technol.*, **99**, 28-35.
- Wu, F.-C., Tseng, R.-L. and Juang, R.-S. (2000), "Comparative adsorption of metal and dye on flake-and bead-types of chitosans prepared from fishery wastes", *J. Hazard. Mater.*, **73**(1), 63-75.
- Xu, X., Deng, C., Gao, M., Yu, W., Yang, P. and Zhang, X. (2006), "Synthesis of magnetic microspheres with immobilized metal ions for enrichment and direct determination of phosphopeptides by matrix-assisted laser desorption ionization mass spectrometry", *Adv. Mater.*, **18**(24), 3289-3293.
- Xu, Y., Zhou, Y., Ma, W., Wang, S. and Li, S. (2013), "Functionalized magnetic core-shell Fe₃O₄@SiO₂ nanoparticles for sensitive detection and removal of Hg²⁺", *J. Nanopart. Res.*, **15**(6), 1-9.
- Zhang, G., Qu, J., Liu, H., Cooper, A.T. and Wu, R. (2007), "CuFe₂O₄/activated carbon composite: a novel magnetic adsorbent for the removal of acid orange II and catalytic regeneration", *Chemosphere*, **68**(6), 1058-1066.
- Zhao, X., Shi, Y., Wang, T., Cai, Y. and Jiang, G. (2008), "Preparation of silica-magnetite nanoparticle mixed hemimicelle sorbents for extraction of several typical phenolic compounds from environmental water samples", *J. Chromatogr. A*, **1188**(2), 140-147.
- Zhong, L.-S., Hu, J.-S., Cao, A.-M., Liu, Q., Song, W.-G. and Wan, L.-J. (2007), "3D flowerlike ceria micro/nanocomposite structure and its application for water treatment and CO removal", *Chem. Mater.*, **19**(7), 1648-1655.